Numerical Simulation on Mode Transition of Atmospheric Dielectric Barrier Discharge in Helium–Oxygen Mixture

Dongsoo Lee, Jin Myung Park, Sang Hee Hong, *Member, IEEE*, and Yongho Kim, *Member, IEEE*

***Abstract*—A one-dimensional numerical simulation of a homogeneous dielectric barrier discharge has been carried out for a nonequilibrium helium–oxygen mixture plasma to understand the influences of oxygen additive on its discharge characteristics at atmospheric pressure. The numerical results obtained by solving continuity equations for plasma species and Poisson equation show that, depending on the amount of oxygen added, the homogeneous barrier discharge turns out to have two fundamental modes: glow and Townsend. When oxygen is rare, the discharge has similar characteristics to the direct current glow discharge at low pressure. As the oxygen additive increases, the discharge characteristics of the glow mode are destroyed and changed into the Townsend mode. The reason for this mode transition is due to the fact that oxygen plays an important role both in quenching helium metastables and in attaching electrons on it in the plasma. As a practical method of sustaining the glow mode even with high oxygen concentration in the discharge, adjustment of the frequency of applied driving voltage is introduced. The numerical simulation reveals that the glow mode recovers from the Townsend mode by increasing the frequency while the amount of oxygen is highly contained. Finally, discharge operation regimes for the glow and Townsend modes are numerically obtained, which are dependent on both oxygen additive and applied frequency.**

***Index Terms*—Atmospheric helium, dielectric barrier discharge, glow mode, numerical simulation, oxygen additive, Townsend mode.**

I. Introduction

THE DIELECTRIC barrier discharge (DBD), which has been traditionally used for ozone generation, is one of the most important nonequilibrium plasma sources at atmospheric pressure [1]. Although the DBD usually generates spatially nonuniform streamers [2], it has been reported that the DBD could produce a homogeneous glow plasma experimentally at certain conditions: with helium discharge gas and/or in high frequency (a few kilohertz) discharge operation [3]–[5]. And some numerical studies on the homogeneous DBD have been also carried out to understand its discharge mechanism [5]–[8]. This homogeneous DBD is very useful especially for the surface treatment of materials and the sterilization process taking advantage of its uniform plasma characteristics [9]–[11].

Manuscript received August 17, 2004; revised December 8, 2004.

D. Lee, J. M. Park, and S. H. Hong are with the Department of Nuclear Engineering, Seoul National University, Seoul 151-742, Korea (e-mail: hongsh@snu.ac.kr).

Y. Kim is with the Plasma Physics Group, Los Alamos National Laboratory, Los Alamos, NM 87545 USA.

Digital Object Identifier 10.1109/TPS.2005.844493

As for the discharge characteristics of DBD, recent numerical work has reported that the homogeneous barrier discharge in helium at atmospheric pressure has two different discharge modes: glow mode and Townsend mode [6], [12], [13]. The homogeneous barrier discharge at the glow mode exhibits discrete discharge structures that are similar to those of direct current (dc) glow discharges at low pressures, and it is usually called the atmospheric pressure glow discharge (APGD). On the other hand, the barrier discharge at the Townsend mode does not have a quasi-neutral region but a positively charged space region. Electric field is not greatly changed within the discharge region and both current density and electron density are relatively small compared with those of the glow mode [6]. Meanwhile, lots of DBD applications require oxygen to produce its chemically active species (CAS), such as O and O_3. However, oxygen deteriorates sustenance of the glow mode because it quenches helium metastables and tends to induce electron attachments. Therefore, understanding of the influences of oxygen additive to the helium discharge gas on the discharge mode is essentially needed to sustain the glow mode which has strong electric field, thick sheath region, and particle densities denser than the Townsend mode has.

In this numerical work, a one-dimensional (1-D) numerical model of the homogeneous DBD has been developed for the nonequilibrium helium–oxygen mixture plasma at atmospheric pressure. First, when the oxygen quantity added in helium is very small (about a few ppm), discharge characteristics of the helium APGD are investigated by solving continuity equations and Poisson equation. Next, mode transition of the DBD from the glow mode to the Townsend mode is illustrated by increasing the amount of oxygen additive. Then, the dependence of mode transition of the DBD on both oxygen quantity and driving frequency is discussed for maintaining the glow mode.

II. Numerical Model and Computational Methods

A. Description of Modeling Geometry

A schematic diagram of the DBD reactor considered in this numerical work is depicted in Fig. 1. In this DBD modeling, it is assumed that the discharge region is filled with a helium–oxygen mixture plasma distributed uniformly along the planes parallel to the electrode surface [5], which enables a 1-D approach to be used for the description of theoretical formulation. The 1-D numerical simulation treats the parallel-plate DBD reactor with double dielectric barriers of $a = 0.1$ cm in thickness. The barriers cover two electrodes at $x = -0.1$ cm and $x = 0.4$ cm,

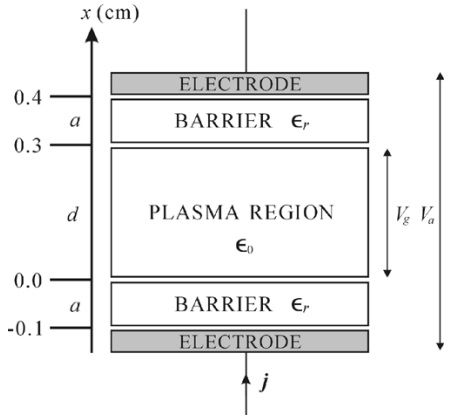

Fig. 1. Schematic diagram of the 1-D DBD simulation model for a parallel-plate DBD reactor with double dielectric barriers.

respectively, and are separated by a plasma region of which gap distance d is 0.3 cm. The dielectric barrier material is alumina (Al_2O_3) with a relative permittivity ε_r of 8.0.

B. Governing Equations

The physical properties of electrons, ions, and neutral species of helium and oxygen are described by the following 1-D continuity equations [14]:

$$\frac{\partial n_k}{\partial t} + \frac{\partial}{\partial x}(n_k v_k) = S_k \tag{1}$$

$$v_k = \mu_k E \tag{2}$$

where n_k, v_k, and S_k are the number density, drift velocity, and source-sink term of the k species, respectively. The drift motions of charged particles are determined mainly by their mobility (μ_k) influenced by electric field E since their diffusion motions are relatively negligible in the direction of discharge. In case of neutral particles (e.g., helium metastable), their drift velocity is set to be zero. The electron mobility is obtained from the electron energy distribution function (EEDF) [15]. In this numerical work, the electron mobility is calculated in the range of the reduced electric field from 1 to 100 Td, and its calculated results show a rapid drop from 2100 to 850 $\mathrm{cm}^2/(\mathrm{V}\cdot\mathrm{s})$ for 1 – 10 Td while they gradually increase from 850 to 980 $\mathrm{cm}^2/(\mathrm{V}\cdot\mathrm{s})$ for 10–100 Td. The mobilities of helium ions are chosen as $\mu_{He^+} = 11.2\ \mathrm{cm}^2/(\mathrm{V}\cdot\mathrm{s})$ and $\mu_{He_2^+} = 20.0\ \mathrm{cm}^2/(\mathrm{V}\cdot\mathrm{s})$ [16], [17]. For computing the source-sink term S_k in possible reaction processes, their reaction rate constants are listed in Tables I and II. Elementary processes in the helium plasma given in Table I are based mainly on [6]. In the tables, the rate constants related to electron collision are also calculated from EEDF, which is explained in Section II-D. In Table I, He^* represents the excited helium combined in two metastable states of $He(2^1S)$ and $He(2^3S)$, and $He_2{}^*$ is a simplified form of the helium excimer molecule $He_2(a^3\Sigma_u{}^+)$. Initial values of electron density, helium metastable density (He^*), and helium excimer molecule density ($He_2{}^*$) are all taken as 10^3 cm^{-3} as the seed particles for discharge ignition. Initial densities of the two helium ions (He^+, $He_2{}^+$) are half the value of the electron density for charge neutrality. Initial oxygen density is varied according to oxygen additive conditions and other densities of the oxygen-related particles are set to vanish. All of these particles are assumed to be distributed uniformly throughout the discharge region.

TABLE I
ELEMENTARY REACTION PROCESSES IN HELIUM DISCHARGE

Reaction	Rate constant k	Reference
$He + e \rightarrow He^+ + 2e$	f(E/N)	[15]
$He + e \rightarrow He(2^1S) + e$	f(E/N)	[15]
$He + e \rightarrow He(2^3S) + e$	f(E/N)	[15]
$He_2{}^+ + e \rightarrow He^* + He$	8.9×10^{-9} $\mathrm{cm}^3\mathrm{s}^{-1}$	[6]
$He_2{}^* + M \rightarrow 2He + M$	1.0×10^{6} s^{-1}	[6]
$He_2{}^* + He_2{}^* \rightarrow He_2{}^+ + 2He + e$	1.5×10^{-9} $\mathrm{cm}^3\mathrm{s}^{-1}$	[18]
$He^* + 2He \rightarrow He_2{}^* + He$	2.0×10^{-34} $\mathrm{cm}^6\mathrm{s}^{-1}$	[18]
$He^* + He^* \rightarrow He_2{}^+ + e$	1.5×10^{-9} $\mathrm{cm}^3\mathrm{s}^{-1}$	[18]

TABLE II
ADDITIONAL REACTION PROCESSES IN THE PRESENCE OF OXYGEN ADDITIVE IN HELIUM DISCHARGE

Reaction	Rate constant k	Reference
$O_2 + e \rightarrow O_2{}^+ + 2e$	f(E/N)	[15]
$O_2 + e \rightarrow O_2{}^-$	f(E/N)	[15]
$O_3 + O \rightarrow O_2 + O_2$	8.30×10^{-15} $\mathrm{cm}^3\mathrm{s}^{-1}$	[19]
$O_2{}^+ + e \rightarrow O + O$	4.8×10^{-7} $\mathrm{cm}^3\mathrm{s}^{-1}$	*
$O_2 + O^+ \rightarrow O_2{}^+ + O$	2.0×10^{-11} $\mathrm{cm}^3\mathrm{s}^{-1}$	[20]
$He^* + O_2 \rightarrow He + O_2{}^+ + e$	2.4×10^{-10} $\mathrm{cm}^3\mathrm{s}^{-1}$	[21]
$He^* + O \rightarrow He + O^+ + e$	4.3×10^{-10} $\mathrm{cm}^3\mathrm{s}^{-1}$	[22]
$He + O + O \rightarrow He + O_2$	1.04×10^{-33} $\mathrm{cm}^6\mathrm{s}^{-1}$	[19]
$He + O_2 + O \rightarrow He + O_3$	6.27×10^{-34} $\mathrm{cm}^6\mathrm{s}^{-1}$	[19]
$He + O_3 \rightarrow He + O_2 + O$	2.28×10^{-26} $\mathrm{cm}^3\mathrm{s}^{-1}$	[19]

* Reaction rate has to be calculated from the EEDF, but a constant value is used in this work for the sake of simplicity.

A rational cubic interpolated propagation (RCIP) scheme is employed to solve the continuity equations numerically and to minimize the numerical diffusions in their solutions [23]. The following Poisson equation (3) for the electric potential ϕ is used for calculation of the electric field E and solved by the second-order finite difference method (FDM) and the tridiagonal matrix algorithm (TDMA):

$$\nabla\cdot(\varepsilon\nabla\phi) = -e(n_i - n_e) \tag{3}$$

$$E = -\nabla\phi \tag{4}$$

where e is the electron charge, n_e and n_i are the densities of electron and positive ion, respectively, and ε means the dielectric permittivity.

The electric current density j in the discharge region is found by Sato's equation with the time-dependent applied voltage [24]:

$$j = \frac{e}{d}\int_0^d (n_i v_i - n_e v_e)dx + \frac{\varepsilon_0}{d}\frac{\partial V_a}{\partial t} \tag{5}$$

where ε_0 is the permittivity of free space and V_a is the applied voltage. The contribution of negative ions to the current is not included here.

C. Boundary Conditions at the Plasma-Barrier Interfaces

The total electron flux $n_e v_e$ coming out from the cathode barrier can be assumed to be equal to the sum of secondary emission flux generated by incoming ions and electron desorption flux from the barrier [25]:

$$n_e v_e = \gamma_i n_i v_i + \nu_{de}\sigma_e \tag{6}$$

where γ_i is the secondary emission coefficient on the barrier, ν_{de} is the electron desorption frequency, and σ_e is the electron surface charge density. In this numerical modeling, γ_i is assumed to be 0.01 and ν_{de} is 10 s^{-1} [6]. Secondary emissions by the photo-effect are not considered in this work where all the metal electrodes are covered with dielectric barriers. The process of photoemission from the dielectric surfaces is negligibly small for atmospheric-pressure helium plasma, because most of the photons are in the visible range, as in the case of nitrogen [25], and their energy is too small to emit the electrons. Secondary emissions by the metastables are also found to be unimportant in the previous work [12], [25]. Therefore, secondary emissions by the metastables and photon fluxes are neglected.

At the plasma-barrier interfaces, the surface charges of positive ion and electron are assumed to be accumulated by the incoming ion and electron fluxes from the plasma region and dissipated by the recombination process between themselves [25]. And the electron desorption from the barrier to the plasma is also suggested as a loss mechanism of electron surface charges. As a result, the surface charge densities of electron and ion (σ_e and σ_i) are expressed as follows:

$$\frac{\partial \sigma_e}{\partial t} = n_e v_e - \nu_{de}\sigma_e - \alpha_{re}\sigma_i\sigma_e \tag{7}$$

$$\frac{\partial \sigma_i}{\partial t} = (1+\gamma_i) n_i v_i - \alpha_{re}\sigma_i\sigma_e \tag{8}$$

where α_{re} ($= 10^{-6}$) is the ion-electron recombination coefficient. Charge losses to the electrodes through the barriers by conduction are not considered here because the barrier material we used is alumina which has an extremely low electrical conductivity ($\sigma < 10^{-12}$ S/cm).

For solving the Poisson equation (3), the boundary condition at the plasma-barrier interfaces needs to be carefully exercised because of variance in the dielectric constant and surface charges accumulated on the barriers. Applying the Gauss theorem to (3) at the interface, the boundary condition is derived in the following 1-D form:

$$\frac{d\phi}{dx} - \varepsilon_r \frac{d\phi_D}{dx} = \frac{e}{\varepsilon_0}(\sigma_i - \sigma_e) \tag{9}$$

where ϕ and ϕ_D are the electric potentials on the plasma and dielectric barrier sides, respectively. Initial values of the surface charge densities (σ_e and σ_i) are taken as 10^{-9} cm^{-2} at the both sides of the barriers.

D. Boltzmann Equation Solver for EEDF

In weakly ionized gases, some reaction coefficients, like ionization rate and excitation rate, are not constant values, but are dependent on electric field as electron mobility and diffusion coefficients are. In high-pressure discharges, electrons and ions are assumed to be in equilibrium depending only on the reduced electric field E/N, where N is the neutral particle density, and the equilibrium is directly related to the distribution function $f(E/N, \varepsilon)$ of electron energy ε. This hydrodynamic assumption has been typically used for nonthermal atmospheric plasmas [5], [7], but the general need for taking into account the nonequilibrium nature in the cathode fall region has been recently raised where the electrons have small kinetic energy (about 0.5 eV) that is not enough to reach equilibrium with the high electric field [26], [27]. However, this nonequilibrium nature of the cathode fall region is not included in this study for simplicity. The field-dependent physical coefficients are calculated by using EEDF $f(\varepsilon)$ obtained from the solution of the spatially homogeneous Boltzmann equation:

$$\frac{\partial f}{\partial t} + \frac{e\mathbf{E}}{m}\cdot\nabla_v f = \left(\frac{\partial f}{\partial t}\right)_{\text{collisions}}. \tag{10}$$

The EEDF $f(\varepsilon)$ in this equation is easily found from a numerical Boltzmann equation solver, BOLSIG [15]. The field-dependent reaction coefficients are then evaluated from the following integrals including the electron distribution function $f(\varepsilon)$:

$$k_k = \int \sigma_k(\varepsilon) f(\varepsilon) d\varepsilon \tag{11}$$

$$\mu_e = \frac{1}{3}\sqrt{\frac{2}{m_e}} \int \frac{\varepsilon}{N\sigma(\varepsilon)} \frac{\partial f(\varepsilon)}{\partial \varepsilon} d\varepsilon \tag{12}$$

where k_k and σ_k are the rate coefficient and cross section of k reaction. The evaluated coefficients have been listed in a tabular form according to E/N values, and used for the calculations during the present discharge modeling.

III. Simulation Results and Discussions

A. Helium–Oxygen Atmospheric Pressure Glow Discharge (He-O_2 APGD)

Fig. 2 describes the time evolution of the calculated discharge current density and gas voltage during one and a half cycles of an applied voltage. The figure shows a steady-state situation and it takes three cycles of the applied voltage, i.e., the transient time is 300 μs, to reach this state at 10 kHz. The amount of oxygen concentration is 5 ppm added in helium at atmospheric pressure, which is a very rare additive, and a sinusoidal voltage of 10 kHz with a peak value of 1.5 kV is applied to the DBD reactor. These current and voltage curves show the typical discharge pattern of helium APGD, which has a single current peak in every half cycle of the applied voltage. The present simulation results, a peak current density of 6.4 $\mathrm{mA/cm}^2$ and a rapid drop of gas voltage at the current peak, are very analogous to those obtained in the others' numerical work and experiments on DBD [5]–[7].

The spatial distributions of electric field, electron density, and ion density are plotted in Fig. 3 when the discharge current is in its maximum state at $t = 408.0$ μs. The discharge characteristics shown in Fig. 3 for the He-O_2 APGD have similarities to those appeared in the dc glow discharge at low pressure, and they are distinguished by four discharge regions featuring the typical glow mode. First, a cathode fall region exists where

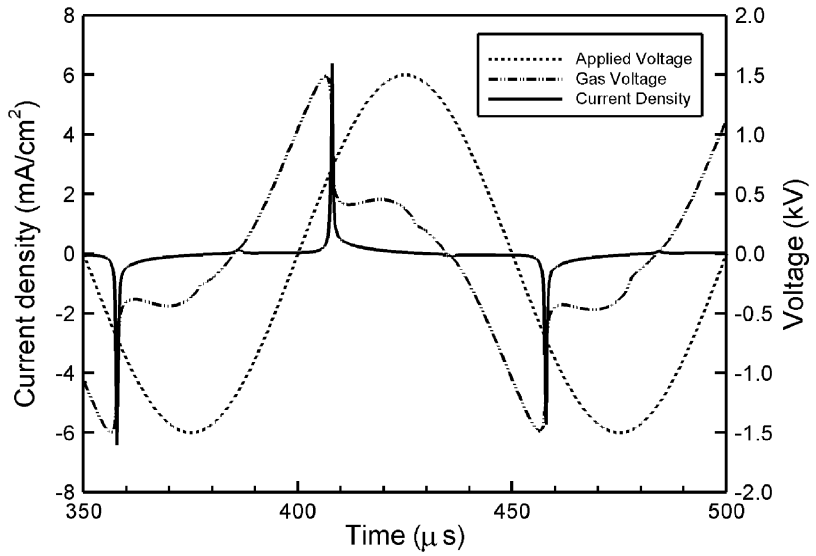

Fig. 2. Time evolution of the calculated discharge current density and gas voltage during one and a half cycles of an applied filed in the helium–oxygen glow mode for oxygen density of 5 ppm and frequency of 10 kHz.

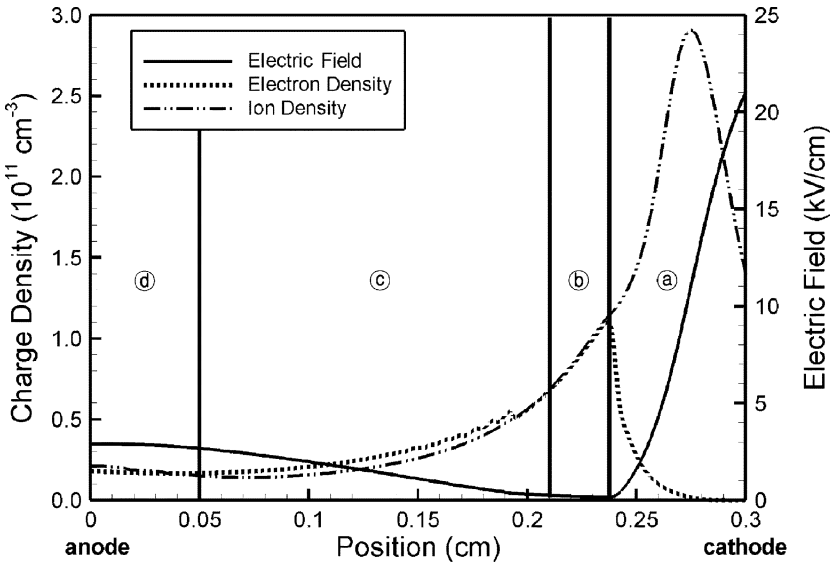

Fig. 3. Spatial distributions of electric field, electron density, and ion density for a phase of maximal current in the glow mode appearing in Fig. 2 (ⓐ : cathode fall, ⓑ: negative glow, ⓒ: Faraday dark space, ⓓ: positive column).

the electric field drops drastically from a maximum value of about 21 kV/cm to nearly zero because of large positive space charges near the cathode. Thickness of the cathode fall is about 0.6 mm and the ion density reaches up to the largest value of 2.9×10^{11} cm^{-3}. Second, a negative glow region extends to 0.3 mm in thickness. In this region, the plasma is nearly quasi-neutral and electron density has its highest value of 1.1×10^{11} cm^{-3}. Third, a Faraday dark space grows to a thickness of 1.6 mm. Electron is more abundant than ion and both electron and ion densities are distributed with low values over the discharge region. Lastly, there is a relatively narrow positive column of 0.5 mm from the anode with electron and ion densities of about 2.0×10^{10} cm^{-3} in a nearly constant field of 3 kV/cm. The origin of the positive column formation in the APGD by an ac voltage operation differs from that in the dc glow discharge in a cylindrical tube reactor at low pressure. The former origin is due to the finite time of the field shielding [6], while the latter is generated because of the recombination of charged particles at the wall of discharge tube [28].

After passing the current peak where the electric field has its highest value during the discharge, the electric field begins to rapidly decrease and the electrons created during this pulse discharge are trapped in the positive column between two major pulse discharges because of the low accelerating field in it. When the polarity of field is reversed, these trapped electrons begin to flow suddenly and induce a small current peak, called "residual current peak" [5]. This residual current peak is also identified by the present numerical work and shown in Fig. 4. This current is a trace of the positive column and an indication that lots of electrons in the discharge gap are reserved sufficiently for producing the next breakdown under the low electric field, and thus for sustaining the APGD.

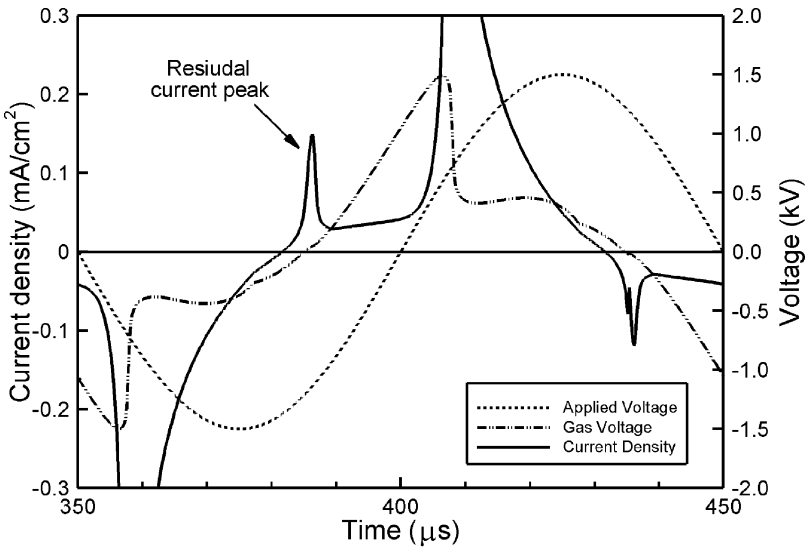

Fig. 4. Residual current peak due to the trapped electrons between two major single discharges. This graph is a magnified figure of Fig. 2.

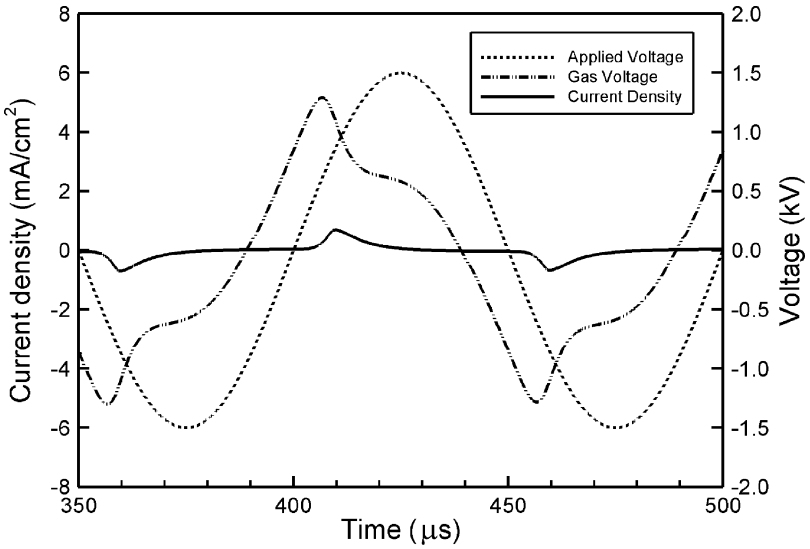

Fig. 5. Time evolution of the calculated discharge current density and gas voltage during one and a half cycles of an applied voltage in the helium–oxygen Townsend mode for oxygen density of 20 ppm and frequency of 10 kHz.

To sum up, the atmospheric pressure helium DBD in the glow mode is considered as a glow discharge in a sense that it has the four distinguishable discharge regions, a large positive space charge exists near the cathode, and secondary electrons are emitted by the cathode-directed ion flux. It is very analogous to the normal dc glow discharge in spite of its operation at atmospheric pressure. Besides, the maximum densities of electron and ion are of the same order as those of the dc glow discharge at low pressure.

B. Effect of Oxygen Additive on DBD Mode Transition

In a pure helium atmosphere, main mechanisms of electron production in the DBD are electron impact ionization and stepwise ionization by the metastable helium. The chemoionization, caused by helium metastable (He^*) and excimer molecule ($\mathrm{He_2}^*$) in Table I, also provides considerable electrons kept in the positive column when the electric field remains low for a period between two major discharges. But in the real discharge situation, there inevitably exist small quantities of other gases in helium because of various causes: impure helium gas supply, imperfect sealing of discharge chamber, etching from the barrier, or intentional addition of reactive gas for effective processing. Thus, impurity effects should be taken into account, and oxygen additive effects among them have been focused in this numerical simulation. Oxygen is known as a very efficient quencher of helium metastables [21], [22], and it destructs helium metastables which play an important role in generating seed electrons by chemoionization to sustain the glow mode. Moreover, oxygen has high electron affinity and attaches electrons easily on it. Therefore, if there is a large amount of oxygen additive, the electrons become deficient in maintaining the glow mode, which will be changed into another discharge mode.

Fig. 5 shows the current and voltage characteristics in the helium–oxygen DBD when oxygen additive is increased to 20 ppm from the previous 5 ppm in Fig. 2 for the glow mode. The frequency of external voltage is kept the same 10 kHz,

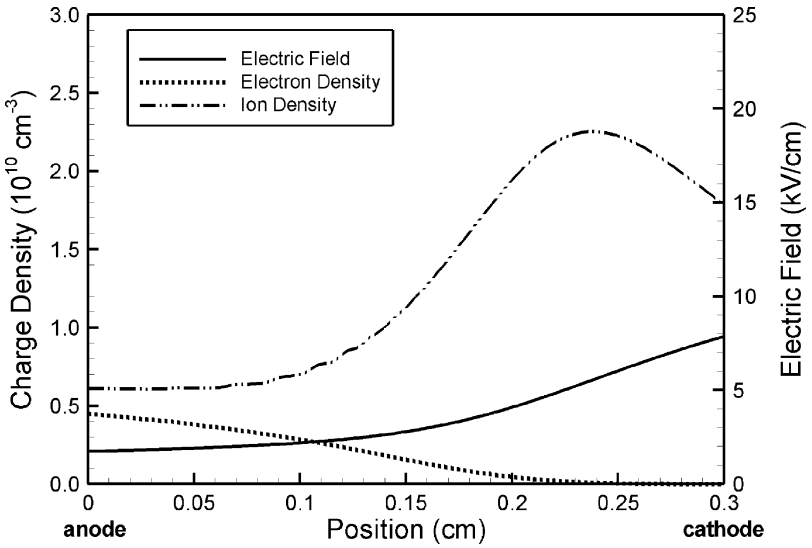

Fig. 6. Spatial distributions of electric field, electron density, and ion density for a phase of maximal current in the Townsend mode appearing in Fig. 5.

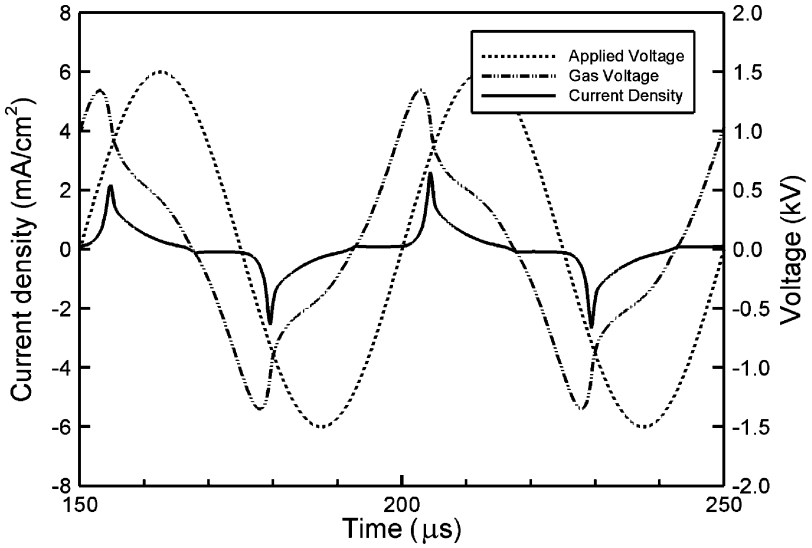

Fig. 7. Time evolution of the calculated discharge current density and gas voltage during two cycles of an applied voltage in the helium–oxygen glow mode for oxygen density of 20 ppm and frequency of 20 kHz.

as in Fig. 2. In this case with increased oxygen content, the gas voltage drops slightly, but the current peak decreases drastically below 1 mA/cm^2 from the previous 6 mA/cm^2 in 5 ppm oxygen. The current profile is not peaked, rather spreads broadly, and the residual current peak is not observed in this case of 20 ppm oxygen.

In order to explain such different discharge characteristics that might be resulted from a transition of the discharge mode, the discharge structures of particles and electric field illustrated in Fig. 6 are analyzed. It is seen from the figure that electron density rises monotonously from the cathode to the anode and its values are about one-tenth of those in the glow mode. On the other hand, ion density exhibits a similar pattern in its spatial distribution to that in the glow mode, but its absolute values are too small to disturb the electric field distribution greatly by the net space charge resulted. All over the discharge region, the ion density exceeds the electron density, so there is no quasi-neutral plasma region like the positive column. The electric field strength is less intense than that of the glow mode and increases gradually from the anode to the cathode. Such physical features can be ascribed to a Townsend discharge and allow to name the mode of this discharge as the Townsend mode [6]. The absence of quasi-neutral region prevents electrons from being trapped in the discharge gas gap, thus the glow mode is not sustained and changed into the Townsend mode. This kind of discharge mode was also predicted in a homogeneous nitrogen DBD at atmospheric pressure [29].

C. Influence of Frequency on DBD Mode Transition

It was pointed out in the previous section that when a large amount of oxygen additive is intentionally added to helium gas, the Townsend mode occurs on account of shortage of the enough electrons trapped in the discharge gas gap during the period between two major discharges where the electric field level is lowered. Helium metastable reduction and electron attachment by the oxygen additive were suggested as the mode

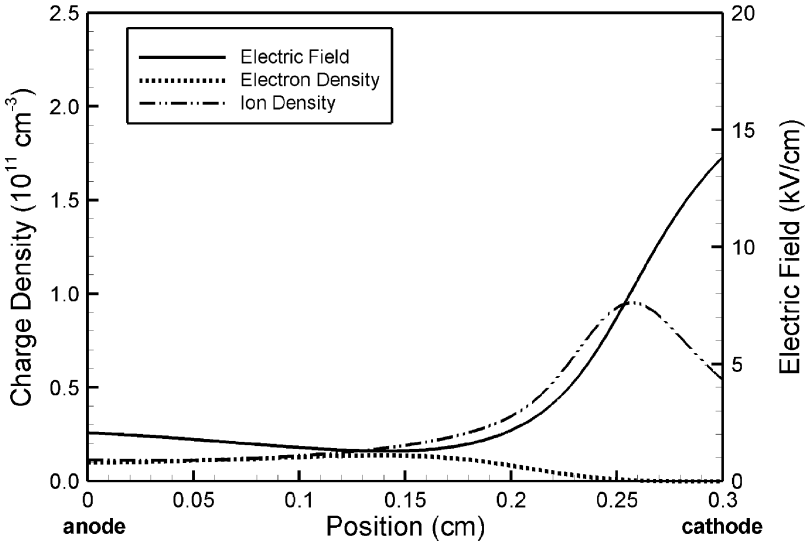

Fig. 8. Spatial distributions of electric field, electron density, and ion density for a phase of maximal current in the glow mode appearing in Fig. 7.

transition mechanism. Then, the glow mode will not be changed into the Townsend mode if it is possible to preserve enough electrons during the nondischarge period. As an approach to the survival of the glow mode, adjustment of the driving voltage frequency for DBD is taken into account in this section. In case the frequency increases or the period between discharges becomes short, the reduction time of helium metastables and the direct attachment of electrons will decrease between the discharge period. Then the electron density will remain sufficient for maintaining the glow mode and the current density will rise again.

The effects of frequency increase on the discharge current and voltage in the He–O_2 DBD are presented in Fig. 7, where the frequency is doubled to 20 kHz from 10 kHz for the Townsend mode in Fig. 5, and the oxygen concentration level still remains at 20 ppm. As the numerical results exhibit in Fig. 7, the discharge current density becomes to have a sharp profile again and its peak value reaches up to about 2.8 mA/cm^2. Furthermore, the residual current peaks appear again. Judging from these current and voltage curves, it is considered that the glow mode is recovered from the Townsend mode by raising the frequency as expected.

To identify the exact mode of this DBD discharge, the spatial structures of particles and field are also analyzed at a current peak. Fig. 8 shows the spatial distributions of particles and field, which have the nearly similar trend to those of the glow mode seen in Fig. 3. The electric field is somewhat differently disturbed by the net space charge and rises up to 14 kV/cm. On the whole, the densities of ion and electron become of the order of 10^{11} cm^{-3} again. The electron density distribution has the largest value at $x = 0.15$ cm without growing monotonously from the cathode to the anode, which is apparently different from that in the Townsend mode. And there also exists a quasi-neutral plasma region in the discharge gap. Then, it is summarized from this numerical simulation that the increment of driving frequency reduces the amount of lost electrons which would have collided with the wall or electrodes at low frequencies, and thus enables the He–O_2 DBD to stay in the glow mode in spite of the higher oxygen concentration.

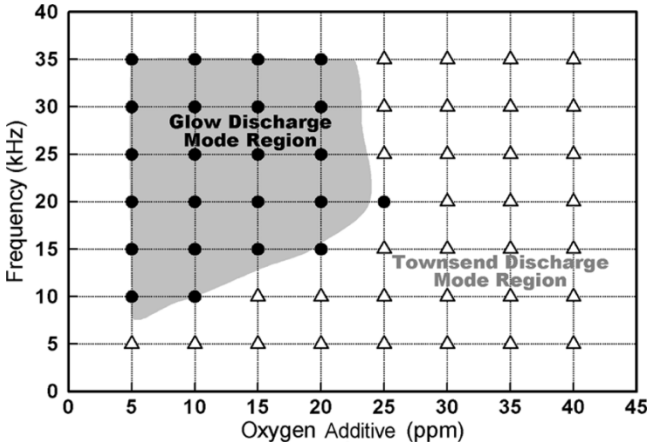

Fig. 9. Discharge mode diagram for identifying the glow (•) and Townsend (△) modes in the helium–oxygen DBD depending on the operation conditions of driving frequency and oxygen additive concentration.

Lastly, the present 1-D numerical simulation has found a discharge operation diagram as given in Fig. 9 for identifying the glow and Townsend modes depending on oxygen additive quantity and driving frequency. The oxygen additive range is varied from 5 to 40 ppm and the frequency range from 5 to 35 kHz. The glow and Townsend mode regions are separated and marked with circles and triangles, respectively. Each discharge mode has been determined from the criteria for the current density profile, the existence of the residual current peak, and the electric field distortion. As revealed in Fig. 9, the minimum frequency for sustaining the glow mode increases linearly with the amount of oxygen additive. But, at more than 25 ppm of oxygen, the glow mode is not obtainable and only Townsend modes exist at any frequencies.

IV. Conclusion

The numerical simulation of homogeneous dielectric barrier discharge in atmospheric pressure helium–oxygen mixture has been performed to analyze its discharge mode transition. The numerical results show that the helium DBD at atmospheric pressure with negligible oxygen additive has similarities to the low-pressure dc glow discharge, and that the helium DBD is, however, transformed into the Townsend mode by increasing the oxygen concentration. As the oxygen additive increases, the discharge characteristics of the glow mode are destroyed and changed into the Townsend mode. This is because oxygen plays an important role both in quenching helium metastables and in attaching electrons on it in the discharge. In order to control this DBD mode transition, the adjustment of driving frequency is suggested in this numerical work as a practical means to sustain the glow mode by suppressing the Townsend mode. The glow mode turns out to be maintained by increasing the applied frequency without changing into the Townsend mode even in the higher oxygen additive concentration. Moreover, from the numerical simulation, a diagram of operating regimes of the glow and Townsend modes is obtained depending on both oxygen concentration and driving frequency. According to this diagram, the maximum oxygen additive to sustain the glow mode is about 25 ppm at 20 kHz. The discharge structures analyzed from the present simulation results reveal that the glow mode has higher electron density, stronger electric field, and thicker sheath region than the Townsend mode. Therefore, the homogeneous helium DBD operated with the glow mode will be very effective for the plasma processing and treatment in its application fields.

References

[1] U. Kogelschatz, B. Eliasson, and W. Egli, "From ozone generators to flat television screens: History and future potential of dielectric-barrier discharges," *Pure Appl. Chem.*, vol. 71, pp. 1819–1828, 1999.

[2] Y. Kim, W. S. Kang, J. M. Park, S. H. Hong, Y. H. Song, and S. J. Kim, "Experimental and numerical analysis of streamers in pulsed corona and dielectric barrier discharges," *IEEE Trans. Plasma Sci.*, vol. 32, no. 1, pp. 18–24, Feb. 2004.

[3] S. Kanazawa, M. Kogoma, T. Moriwaki, and S. Okazaki, "Stable glow plasma at atmospheric pressure," *J. Phys. D, Appl. Phys.*, vol. 21, pp. 838–840, 1988.

[4] J. R. Roth, P. P. Tsai, C. Liu, M. Laroussi, and P. D. Spence, "One Atmosphere Uniform Glow Discharge Plasma," U.S. Patent 5 414 324, May 9, 1995.

[5] F. Massines, A. Rabehi, P. Decomps, R. B. Gadri, P. Ségur, and C. Mayoux, "Experimental and theoretical study of a glow discharge at atmospheric pressure controlled by dielectric barrier," *J. Appl. Phys.*, vol. 83, pp. 2950–2957, 1998.

[6] Y. B. Golubovskii, V. A. Maiorov, J. Behnke, and J. F. Behnke, "Modeling of the homogeneous barrier discharge in helium at atmospheric pressure," *J. Phys. D, Appl. Phys.*, vol. 36, pp. 39–49, 2003.

[7] M. G. Kong and X. T. Deng, "Electrically efficient production of a diffuse nonthermal atmospheric plasma," *IEEE Trans. Plasma Sci.*, vol. 31, no. 1, pp. 7–18, Feb. 2003.

[8] R. B. Gadri, "One atmosphere glow discharge structure revealed by computer modeling," *IEEE Trans. Plasma Sci.*, vol. 27, no. 1, pp. 36–37, Feb. 1999.

[9] S. F. Miralaï, E. Monette, R. Bartnikas, G. Czeremuszkin, M. Latrèche, and M. R. Wertheimer, "Electrical and optical diagnostics of dielectric barrier discharge (DBD) in He and N_2 for polymer treatment," *Plasmas Polym.*, vol. 5, pp. 63–77, 2000.

[10] F. Massines, N. Gherardi, and F. Sommer, "Silane-based coatings on polypropylene, deposited by atmospheric pressure glow discharge plasmas," *Plasmas Polym.*, vol. 5, pp. 151–172, 2000.

[11] T. C. Montie, K. Kelly-Wintenberg, and J. R. Roth, "An overview of research using the one atmosphere uniform glow discharge plasma (OAUGDP) for sterilization of surfaces and materials," *IEEE Trans. Plasma Sci.*, vol. 28, no. 1, pp. 41–50, Feb. 2000.

[12] L. Mangolini, C. Anderson, K. Sittig, P. Zhang, M. Hur, J. Heberlein, and U. Kortshagen. Effects of current limitation through the dielectric in atmospheric pressure glows in helium. presented at Proc. 16th Int. Symp. Plasma Chemistry. [CD-ROM]

[13] F. Massines, P. Ségur, N. Gherardi, C. Khamphan, and A. Ricard, "Physics and chemistry in a glow dielectric barrier discharge at atmospheric pressure: Diagnostics and modeling," *Surf. Coatings Technol.*, vol. 174–175, pp. 8–14, 2003.

[14] W. S. Kang, J. M. Park, Y. Kim, and S. H. Hong, "Numerical study on influences of barrier arrangements on dielectric barrier discharge characteristics," *IEEE Trans. Plasma Sci.*, vol. 31, no. 4, pp. 504–510, Aug. 2003.

[15] BOLSIG. KINEMA Software. [Online]. Available: http://www.siglo-kinema.com

[16] D. Smith and M. J. Copsey, "Investigation of the helium afterglow: I. Mass spectrometric observations," *J. Phys. B, At. Mol. Opt. Phys.*, vol. 1, pp. 650–659, 1968.

[17] Y. B. Golubovskii, V. A. Maiorov, J. Behnke, and J. F. Behnke, "Influence of elementary processes over a homogeneous barrier discharge in helium," in *Proc. Int. Symp. High Pressure Low Temp. Plasma Chem. (HAKONE VIII)*, Pühajärve, Estonia, Jul. 2002, pp. 48–52.

[18] R. Deloche, P. Monchicourt, M. Cheret, and F. Lambert, "High-pressure helium afterglow at room temperature," *Phys. Rev. A, Gen. Phys.*, vol. 13, pp. 1140–1176, 1976.

[19] J. Y. Jeong, J. Park, I. Henins, S. E. Babayan, V. J. Tu, G. S. Selwyn, G. Ding, and R. F. Hicks, "Reaction chemistry in the afterglow of an oxygen-helium, atmospheric-pressure plasma," *J. Phys. Chem. A*, vol. 104, pp. 8027–8032, 2000.

[20] A. B. Rakshit, H. M. P. Stock, D. P. Wareing, and N. D. Twiddy, "Some ion-molecule reaction rate coefficient measurements at 300 and 100 K in a temperature-variable flowing-afterglow apparatus," *J. Phys. B, At. Mol. Opt. Phys.*, vol. 11, pp. 4237–4247, 1978.

[21] W. Lindinger, A. L. Schmeltekopf, and F. C. Fehsenfeld, "Temperature dependence of de-excitation rate constants of $He(2^3S)$ by Ne, Ar, Xe, H_2, N_2, O_2, NH_3, and CO_2," *J. Chem. Phys.*, vol. 61, pp. 2890–2895, 1974.

[22] K. L. Bell, A. Dalgarno, and A. E. Kingston, "Penning ionization by metastable helium atoms," *J. Phys. B, At. Mol. Opt. Phys.*, vol. 1, pp. 18–22, 1968.

[23] F. Xiao, T. Yabe, and T. Ito, "Constructing oscillation preventing scheme for advection equation by rational function," *Comp. Phys. Commun.*, vol. 93, pp. 1–12, 1996.

[24] R. Morrow and N. Sato, "The discharge current induced by the motion of charged particles in time-dependent electric fields; Sato's equation extended," *J. Phys. D, Appl. Phys.*, vol. 32, pp. L20–L22, 1999.

[25] Y. B. Golubovskii, V. A. Maiorov, J. Behnke, and J. F. Behnke, "Influence of interaction between charged particles and dielectric surface over a homogeneous barrier discharge in nitrogen," *J. Phys. D, Appl. Phys.*, vol. 35, pp. 751–761, 2002.

[26] X. Yuan and L. L. Raja, "Computational study of capacitively coupled high-pressure glow discharges in helium," *IEEE Trans. Plasma Sci.*, vol. 31, no. 4, pp. 495–503, Aug. 2003.

[27] J. J. Shi and M. G. Kong, "Cathode fall characteristics in a dc atmospheric pressure glow discharge," *J. Appl. Phys.*, vol. 94, pp. 5504–5513, 2003.

[28] Y. P. Raizer, *Gas Discharge Physics*. Berlin, Germany: Springer-Verlag, 1991, pp. 193–199.

[29] P. Ségur and F. Massines, "The role of numerical modeling to understand the behavior and to predict the existence of an atmospheric pressure glow discharge controlled by a dielectric barrier," in *Proc. 13th Int. Conf. Gas Discharges Appl.*, Glasgow, U.K., Sep. 2000, pp. 15–24.

Dongsoo Lee was born in Busan, Korea, in 1976. He received the B.S and M.S. degrees in nuclear engineering from Seoul National University, Seoul, Korea, in 1999 and 2004, respectively. He is currently working toward the Ph.D. degree in Department of Engineering Physics, the University of Wisconsin, Madison.

His research interests are focused on the atmospheric pressure barrier discharge and plasma etching with low pressure nonequilibrium plasmas.

Jin Myung Park was born in Seoul, Korea, in 1972. He received the B.S., M.S., and Ph.D. degrees in nuclear engineering from Seoul National University, Seoul, Korea, in 1996, 1998, and 2005, respectively

In 2005, he joined the Korea Basic Science Institute, Daejeon, Korea. His research interests include the tokamak plasma transport in nuclear fusion and numerical simulations of dc arc plasmas and pulsed corona discharges.

Sang Hee Hong (M'87) received the B.S. degree in applied physics from Seoul National University (SNU), Seoul, Korea, in 1974 and the M.S. and Ph.D. degrees in electrical engineering from Colorado State University, Fort Collins, in 1975 and 1978, respectively.

In 1979, he joined the College of Engineering, SNU, where he is currently a Professor of nuclear engineering. He spent a year at the University of Sydney, Sydney, Australia, in 1989 as a Visiting Professor. His research interests in the U.S. and Australia were stability analysis of MHD flows and theory of rotating plasma and plasma centrifuges. His research interests in Korea moved to numerical modeling of tokamak plasma and industrial processing plasmas. Recently, his efforts have been concentrated on tokamak plasma modeling and development of thermal plasma sources, such as dc and RF plasma torches, and pulsed corona and dielectric barrier discharge reactors, as well as their materials and environmental processing.

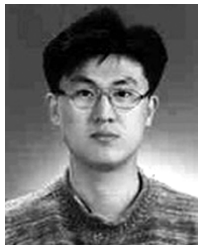

Yongho Kim (M'03) was born in Yeasan, Korea, in 1970. He received the B.S., M.S., and Ph.D. degrees in nuclear engineering from Seoul National University, Seoul, Korea, in 1994, 1996, and 2002, respectively.

In 2002, he joined the Korea Institute of Machinery and Materials, Daejeon, Korea, where he worked on the streamer dynamics generated by pulsed corona and dielectric barrier discharges. He is currently a Postdoctoral Researcher with the Plasma Physics Group (P-24), Los Alamos National Laboratory, Los Alamos, NM. His research interests include the plasma etching with atmospheric pressure plasma jet, plasma assisted combustion, and plasma assisted fuel reformation.